공학석사 학위논문

In-Situ Preparation of Graphene/Carbon Nanotube/Poly(styrenesulfonic acid-*graft*-polyaniline) Nanocomposite *via* Direct Exfoliation of Graphite for Supercapacitor Application

흑연의 직접 박리를 통한 그래핀/카본나노튜브/**S–*g*–A** 나노복합재료 연속적 합성 및 슈퍼커패시터로써 활용

2016년 2월

서울대학교 대학원

재료공학부

이 진 우

Abstract

In-Situ Preparation of Graphene/Carbon Nanotube/Poly(styrenesulfonic acid-*graft*-polyaniline) Nanocomposite *via* Direct Exfoliation of Graphite for Supercapacitor Application

Lee, Jin Woo

Department of Materials Science and Engineering

Seoul National University

Graphene/carbon nanotube/poly(styrenesulfonic acid-*graft*-aniline) (Gr/CNT/S-*g*-A) composites are prepared through direct exfoliation of graphite using S-*g*-A as a surfactant. Compared with other fabrication methods of graphene/CNT/polyaniline composites such as in-situ polymerization and electrochemical polymerization, the direct exfoliation method yields higher quality of graphene, because graphite is directly used as a precursor for graphene without chemical treatment. The in-situ prepared nanocomposite of Gr/CNT/S-*g*-A exhibits a superior specific capacitance of 531 F/g at a current density of 0.5 A/g, which is one of the highest values among supercapacitor electrodes based on graphene/CNT/polyaniline composites. This high value of specific capacitance is attributed to taking both advantages of high specific area of graphene and CNT and high pseudocapacitance of polyaniline.

Keywords: graphene, polyanilne, carbon nanotube, supercapacitor, direct exfoliation

Student Number: 2014-21438

Contents

List of Schemes

List of Figures

List of Tables

1. Introduction

Emerging need for portable electronic devices and electric vehicles has motivated us to discover and develop new class of energy-storage system. Among various energy-storage systems, supercapacitor has attracted much attention due to their high power density, long cycle life and fast charge/discharge rate.[1–4] Supercapacitor can be classified into two categories based on the energy storage mechanism: electrical double-layer capacitor (EDLC) and pseudocapacitor.[3] Carbon nanomaterials with high surface area are mostly used for fabrication of EDLC, and the capacitance comes mainly from charge separation and accumulation at the electrode/electrolyte interface. On the other hand, pseudocapacitor stores the energy by reversible redox reaction of electro-active conducting polymer or transition metal, which acts

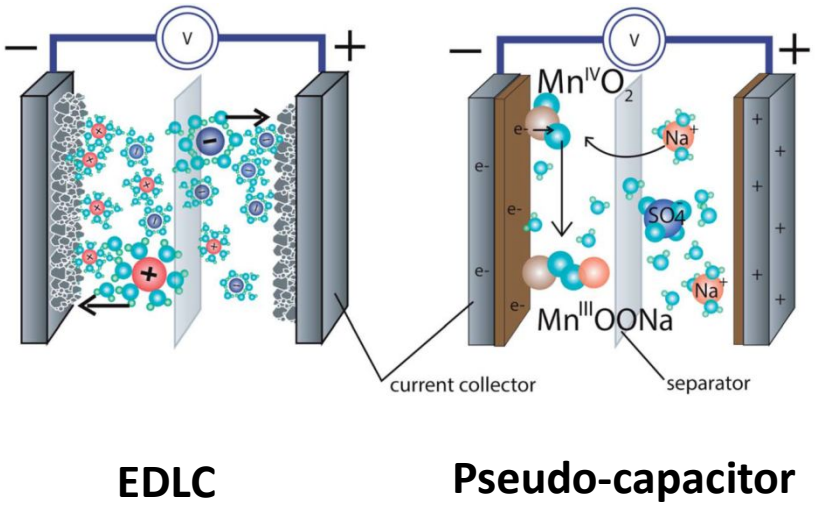

Figure 1.1 Types of supercapacitor

as electrode material.[3,5] Although the transition metal oxides such as ruthenium oxide and cobalt oxide exhibit high capacitance due to their unique redox reaction, they can be readily broken under mechanical stress without flexibility, which limits their use as the supercapacitor electrode in flexible electronic equipment.[6]

Graphene[7,8], a single atomic layer of carbon atoms arranged in a hexagonal honeycomb structure, has continued to attract a good deal of attention due to its superb electric, optical, thermal, mechanical properties[9-11]. Despite intense interest and continuing experiments, widespread implementation of grapheme production has yet to occur. Even though the original bottom-up production of graphene (eg. chemical vapor deposition) is common, there are some difficulties in terms of money and time cost.

Carbon nanotube (CNT) can be constructed by wrapping up a graphene cylindrically. CNTs, according to the concentric graphene sheets, can be classified into two types: Single walled carbon nanotube (SWCNT) and multi-walled carbon nanotube (MWCNT). SWCNT wrapped up by single layer graphene is the fundamental form of CNT. Meanwhile, MWCNT consist of several graphene sheets coaxially arranged around a central hollow core. These two carbon materials are the most commoly used materials for supercapacitor electrode as EDLC type due to their high conductivities and large surface areas.

Polyaniline (PANI) is one of the most promising materials for supercapacitor electrode because of its high capacitance by multiple redox reactions, environmental stability, low cost and easy synthesis.[12,13] Although

the theoretical capacitance of PANI-based supercapacitor reaches up to 2000 F/g,[9] the main limitation, which restricts the use of PANI as electrode material, is low cycle life due to mechanical degradation during charge/discharge process.[15] For the purpose to sustain high capacitance for long-term cycling, the composites of PANI and carbon nanomaterial (e.g., graphene) have been developed because the composite can take both advantages of high surface area of graphene and CNT and outstanding capacitance of PANI, and consequently exhibits high capacitance without serious degradation of PANI.[16]

Most of graphene/CNT/PANI composites as supercapacitor electrode have been synthesized *via* in-situ polymerization,[12] and electrochemical polymerization[19] of aniline in the presence of graphene oxide (GO) and CNT. However, these methods have inherent shortcomings including long reaction time, additional reaction steps and inferior electrochemical properties of graphene sheets reduced from GO which can be comfirmed through raman spectroscopy.[20,21] Therefore, it is necessary to develop simpler and more facile method to fabricate high performance electrode materials for supercapacitor.

Direct exfoliation of graphite into graphene by surfactant and its dispersion in various solvents have been reported: Lotya et al.[22] reported exfoliation of graphite in aqueous media using sodium dodecyl benzene sulfonate for the first time. Later, An et al.[20] have developed stable aqueous dispersion of graphene using 1-pyrenecarboxylic acid (PCA) as a surfactant, in which pyrene moiety can be adsorbed on the graphene surface *via* $\pi-\pi$ interaction and carboxyl acid group facilitates the dispersion of graphene in

polar solvents. However, the supercapacitor electrode based on graphene exfoliated by PCA shows a moderate specific capacitance of 120 F/g since it only used graphene as supercapacitor electrode for saving charges.

Herein, we report the preparation of graphene/carbon nanotube/poly(styrenesulfonic acid-graft-aniline) (Gr/CNT/S-*g*-A) nanocomposite by direct exfoliation of graphite and its application for supercapacitor electrode. Although PANI has strong π–π interaction with graphene sheet, its poor solubility in common solvent makes it difficult to use PANI as a surfactant for exfoliating graphite into graphene layers. Hence, we synthesized and used a water soluble and self-doped conducting polyaniline graft copolymer (S-*g*-A)[23] as an effective surfactant for direct exfoliation of graphite, where PANI graft is adsorbed on the graphene surface *via* π–π interaction and poly(styrenesulfonic acid) main chain is soluble in water and common organic solvents.

This method has many advantages over other exfoliation methods: First, this method does not require an extra process for exfoliation of graphite such as oxidation-reduction reaction of graphite, which facilitates production of high quality graphene. Second, the directly exfoliated graphenes have much less defects than those prepared by other exfoliation methods. Third, nanocomposites of graphene, CNT and conducting polymer can be prepared by simply mixing graphite, CNT and conducting polymer in solvent followed by evaporation of solvent. The nanocomposite of Gr/CNT/S-*g*-A exhibits a high specific capacitance of 531 F/g at a current density of 0.5 A/g by taking advantages of both EDLC and pseudocapacitance energy saving mechanisms,

and good cycling stability with 91% retention of the initial capacitance after 5000 cycles. To the best of our knowledge, the specific capacitance of 531 F/g at 0.5 A/g is among the highest value for graphene/CNT/PANI composite supercapacitor electrode. This result clearly demonstrates that the direct exfoliation of graphite and in-situ preparation of graphene/CNT/conducting polymer nanocomposite using soluble conducting polymer provides a new avenue to develop high-performance supercapacitor electrode for energy storage device.

2. Experimental Section

2.1. Materials

Various reagents were purchased from Sigma-Aldrich, Alfa-Aesar, TCI chemicals. Aniline (ACS reagent, ≥99.5%), Sodium 4-vinylbenzenesulfonate (technical, ≥90%), 4-vinylaniline (97%), Graphite and Multi-walled carbon nanotube (MWCNT) were purchased from Sigma-Aldrich.

2.2. Synthesis of S-*g*-A

2.2.1. Synthesis of tert-butyl 4-vinylphenylcatbamete (BOC-AMS)

Scheme 2.1 shows the whole synthesis route of S-*g*-A. A solution of aminostyrene (1.19 g, 10 mmol) in 10 ml of deionized water (H_2O) was added di-tert-butyl dicarbonate (Boc_2, 2.40 g, 11 mmol). After vigorously stirring at 35 °C for 4 hours, the mixture was extracted with dichloromethane (DCM, 25ml). The organic layer was dried by anhydrous sodium sulfate (Na_2SO_4) and filtered. The filtrate was concentrated, and the residue was purified by flash chromatography (FC) (ethyl acetate/hexane = 2/8) to give 2.18 g white solid (yield: 99%). ^{1}H NMR (300 MHz, $CDCl_3$): δ (ppm) 7.34 (s, 4H), 6.67 (dd, 1H, J=10.8 Hz, J=17.6 Hz), 6.47 (br, 1H), 5.66 (d, 1H, J=17.6 Hz), 5.17 (d, 1H, J= 11 Hz), 1.53 (s, 9H).

2.2.2. Synthesis of P(SSNa-co-BOC-AMS)

P(SSNa-co-BOC-AMS) was synthesized by copolymerizing sodium 4-vinylbenzenesulfonate (SSNa) and t-BOC-AMS by using azobisisobutyronitrile (AIBN) as an initiator. SSNa (2.82 g, 13 mmol), t-BOC-AMS (0.15 g, 0.65 mmol), and AIBN (53 mg) were dissolved in 50 ml of dimethyl sulfoxide (DMSO) and polymerized at 80 °C for 15 hours under N_2 atmosphere. After polymerization, the product was precipitated with acetone, filtered, washed several times with acetone, and dried in a vacuum oven at 50 °C for 24 hours. ^{1}H NMR spectra (300 MHz, DMSO-*d*6) show the peak at 1.5 ppm ($-CH_3$).

2.2.3. Synthesis of S-*g*-A

Elimination of the BOC group from P(SSNa-co-BOC-AMS) and ion exchange of Na^+ with H^+ were carried out under acidic conditions. P(SSNa-co-BOC-AMS) (1.0 g) was added to 30 ml of HCl aqueous solution (1 M) at 30 °C for 1 hour under stirring to yield P(SSNa-co-AMS), and then the solution temperature was lowered to 0 °C. For graft copolymerization of aniline (ANI) (0.086 g) was added to the above copolymer solution for 0.5 hours with stirring, and then 20 ml of ammonium persulfate (0.25 g)/HCl aqueous solution (1 M) was dropwise added at 0 °C. After 6 hours of reaction, a dark green solution was obtained and then filtered. The filtered solution was further purified by dialysis using a semipermeable membrane (molecular weight cutoff, 3500). ^{1}H NMR spectra (300 MHz, DMSO-d_6) of S-*g*-A shows

multiple peaks at 7.0, 7.1, 7.2 and 7.3 ppm, which are assigned to hydrogens in phenyl and quinoid rings of PANI. The peak at 1.5 ppm, which is related to $-CH_3$, disappeared because of removing BOC group in 1 M HCl solution.

2.3. Preparation of Gr/S-*g*-A and Gr/CNT/S-*g*-A composites

Various graft copolymers, S-*g*-As, were synthesized, where the molar ratio of ANI to SSA in S-*g*-A was varied from 0.5, 0.7, 0.9 to 1.2. 100 mg of graphite and 100 mg of S-*g*-As (molar ratios of 0.5, 0.7, 0.9, 1.2) were dissolved in 10 ml ethanol *via* bath-type sonication for 8 hours (Gr/S-*g*-A solutions). After the solutions were centrifuged at 2000 rpm for 1 h, Gr/S-*g*-A nanocomposites were prepared by evaporation of solvent. For preparing Gr/CNT/S-*g*-A nanocomposites, 100 mg of MWCNT was also dissolved in 10 ml ethanol with 100 mg of S-*g*-A (molar ratios of 0.5, 0.7, 0.9, 1.2) *via* bath-type sonication for 8 hours (CNT/S-*g*-A solutions). Both of the Gr/S-*g*-A solution which was the state before centrifugation and MWCNT/S-*g*-A solution were put together and dispersed *via* bath-type sonication for 8 hours again. The dispersed solutions were centrifuged at 2000 rpm for 1 h. The supernatants were decanted. Gr/CNT/S-*g*-A nanocomposites were prepared by evaporation of solvent. Gr/CNT/S-*g*-A nanocomposites were dried at 30 °C under vacuum for 24 h.

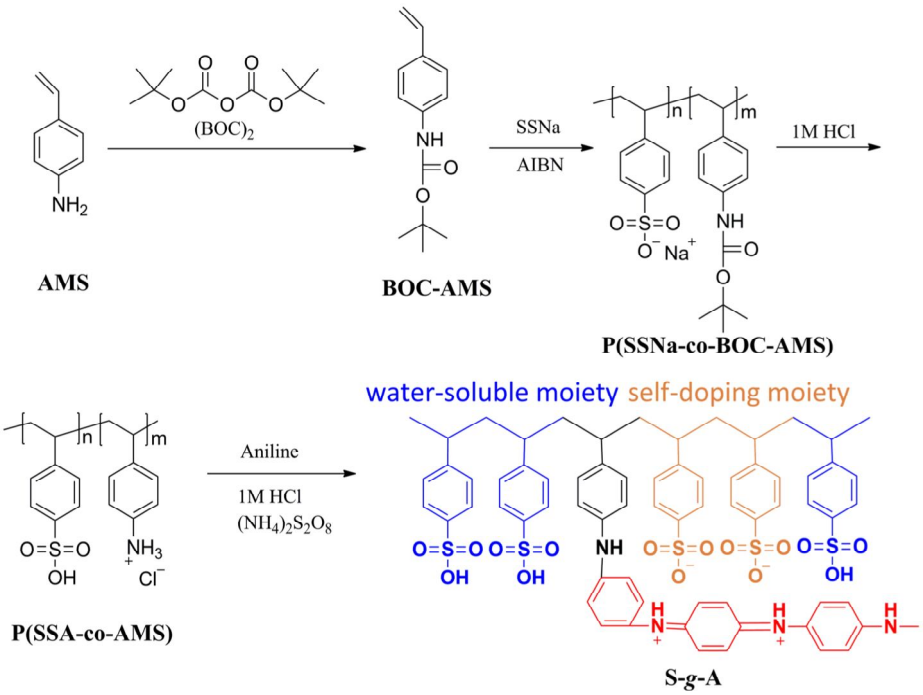

Scheme 2.1 The synthetic scheme of S-*g*-A.

2.4. Measurements

2.4.1. Characterization

The chemical structures were identified by ^{1}H NMR (Avance DPX-300, Bruker). The morphology and microstructure of direct exfoliated graphene in Gr/S-*g*-A composite and Gr/CNT/S-*g*-A composite were characterized by scanning electron microscopy (SEM, SU 70), transmission electron microscopy (TEM, JEOL-3010) and atomic force microscopy (AFM, NANOStation2, Surface imaging systems). Elemental analyses were

recorded with an element analyzer (JMS600w, JEOL) in fast atom bombardment mode. Raman spectra were recorded with a spectrophotometer (Ramanplus, Nanophoton) with an operating wavelength of 514 nm. X-ray photoelectron spectroscopy (XPS) spectra of composites were obtained using an AXIS-HSi spectrometer (KRATOS). The specific surface areas of the composite were determined by the Brunauer-Emmett-Teller (BET) method of nitrogen adsorption at 77 K using a surface area analyzer (ASAP2020, Micromeritics). The electrical conductivities were measured using a four-point probe (Cresbox, NAPSON).

2.4.2. Electrochemical Measurements

The working electrode was prepared by dropping the as-prepared dispersed solutions on the platinum electrode without use of binder. The mass loading of the active materials on the platinum electrode was 50 μg. Electrochemical experiments of electrode materials were carried out by a three-electrode setup in which platinum wire and Ag/AgCl electrode were used as counter electrode and the reference electrode, respectively. A 0.1 M solution of tetrabutylammonium hexafluorophosphate (Bu_4NPF_6) in anhydrous acetonitrile was used as supporting electrolyte. The cyclic voltammetry (CV) and galvanostatic charge/discharge tests were performed with a VMP3 (Bio-Logic) with a scan range of –0.2 to 1.2 V.

The specific capacitance (*Cs*) of the electrode materials can be calculated from the CV curves by the following equation:

$$C_S = (\int IdV) \Big/ (vmV) \quad ,$$

where I is the response current (A), V is the potential (V), v is the potential scan rate (V/s), and m is the mass of the electrode materials (g). The term of $\int IdV$ is calculated from area of CV curves. The specific capacitance (Cs) can also be calculated from the discharge curve according to the following equation:

$$C_S = (I \times \Delta t) \Big/ (\Delta V \times m) \,,$$

where I is the constant discharge current (A), Δt is the discharge time (s), ΔV is the voltage range (excluding the IR drop) (V), and m is the mass of the electrode material (g). Energy density (E) and power density (P) can be calculated from the galvanostatic charge/discharge curves using the following equations:

$$E = \frac{1}{2} CV^2 \quad \text{and} \quad P = \frac{E}{t} \quad ,$$

where C is the specific capacitance calculated from galvanostatic curves, t is the discharge time, ΔV is the voltage range (excluding the IR drop) and m is the mass of the electrode materials.

3. Results and Discussion

3.1. Synthesis and Characterization

The chemical structure of S-*g*-A and direct exfoliation of graphite and dispersion of MWCNT for preparation of Gr/CNT/S-*g*-A nanocomposites are illustrated in Figure 3.1. As illustrated in Figure 3.1, two solutions of graphene/S-*g*-A solution and MWCNT/S-*g*-A solution were prepared separately by bath type sonication. After the preparation, two solutions were mixed together by bath type sonication again. Four S-*g*-A copolymers with different compositions of styrene sulfonic acid (SSA) and aniline (ANI) in copolymer were synthesized. Phenyl ring of aniline is strongly physisorbed onto the basal plane of graphene *via* strong π–π interaction,[24] while hydrophilic sulfonic acid group affords solubility in various solvents such as water, DMSO, methanol and ethanol. First of all, Gr/S-*g*-A nanocomposites were prepared by simply adding graphite flakes and S-*g*-A copolymer into a solvent followed by sonicating the solution using a bath-type sonicator. Among various organic solvents tested, ethanol was the best solvent to exfoliate graphite and to disperse graphene sheets in solvent in the presence of S-*g*-A. To investigate the effect of hydrophilic/phobic ratio of S-*g*-A on exfoliation of graphite, four S-*g*-A copolymers with different molar ratios of ANI to SSA in the copolymer were synthesized, where S-*g*-A(0.5), S-*g*-A(0.7), S-*g*-A(0.9), and S-*g*-A(1.2) denote S-*g*-A with different molar ratios of ANI to SSA (0.5, 0.7, 0.9 and 1.2, respectively). The chemical

structures of tert-Butyl 4-vinylphenylcarbamate, P(SSNa-co-BOC-AMS) and S-*g*-A are identified by ^{1}H NMR as shown in Figure 3.2–4. The molar ratios of ANI to SSA in the copolymers, as determined by elemental analysis, are nearly equal to the molar ratio of ANI to SSA in the feed for polymerization, and the electrical conductivity of copolymer increases with increasing the molar ratio of ANI to SSA (Table 3.1).

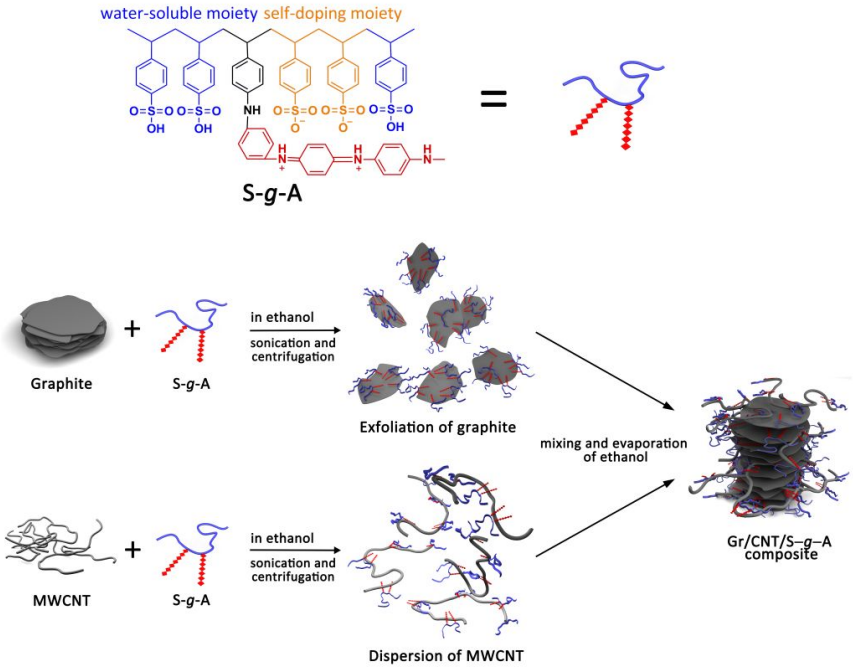

Figure 3.1 The chemical structure of S-*g*-A and schematic illustration of preparation of Gr/CNT/S-*g*-A nanocomposite

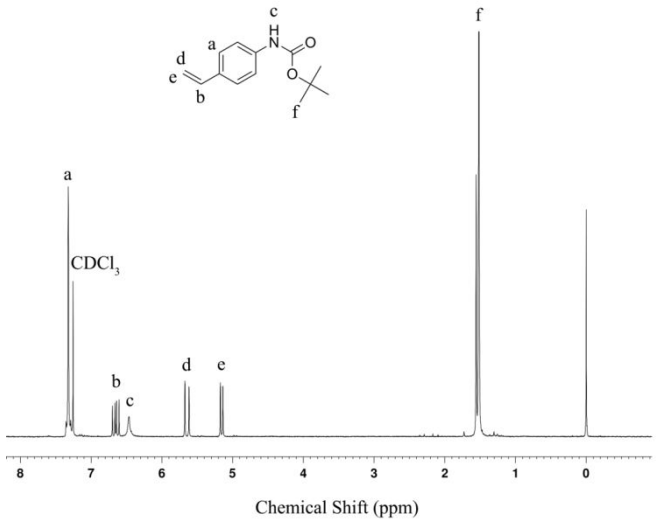

Figure 3.2 Chemical structure and ^{1}H NMR spectrum of tert-butyl 4-vinylphenylcarbamate.

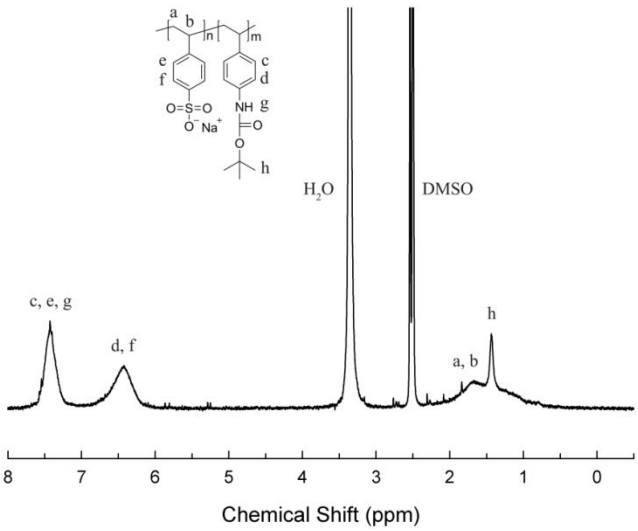

Figure 3.3 Chemical structure and ^{1}H NMR spectrum of P(SSNa-co-BOC-AMS).

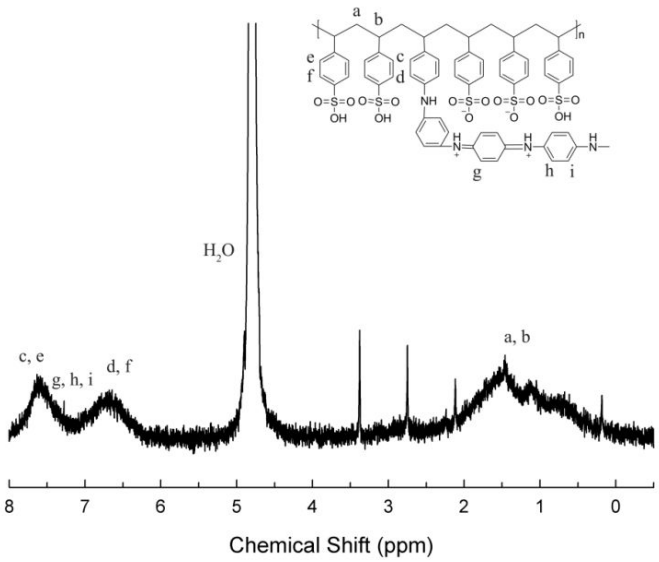

Figure 3.4 Chemical structure and ^{1}H NMR spectrum of S-*g*-A

Table 3.1 Synthesis and electrical conductivities of poly(styrenesulfonic acid-graft-polyaniline) with various ratios of aniline to styrenesulfonic acid.

Sample	Ratio of ANI/SSA in the feed	Ratio of ANI/SSA in copolymer[a]	σ_{elec}[b] (S/cm)
S-*g*-A(0.5)	0.5	0.53	0.62×10^{-1}
S-*g*-A(0.7)	0.7	0.69	0.89×10^{-1}
S-*g*-A(0.9)	0.9	0.88	1.31×10^{-1}
S-*g*-A(1.2)	1.2	1.20	1.49×10^{-1}

[a]Ratio of ANI/SSA in copolymer are determined by elemental analysis; [b]σ_{elec} is electrical conductivity

3.2. Optical images of dispersions of S-*g*-A and it composites

When the dispersions of four S-*g*-A copolymers and the corresponding nanocomposites of Gr/S-*g*-A in ethanol were observed by visual images, three copolymers (S-*g*-A(0.5), S-*g*-A(0.7), and S-*g*-A(0.9)) are soluble in ethanol showing dark green color while S-*g*-A(1.2) with high content of ANI in the copolymer is not soluble (Figure 3.5), and graphene layers in three composites (Gr/S-*g*-A(0.5), Gr/S-*g*-A(0.7), Gr/S-*g*-A(0.9)) are well exfoliated in ethanol while graphene layers in Gr/S-*g*-A(1.2) are aggregated and precipitated at the bottom, implying that higher molar ratio of ANI to SSA over 1.2 results in poorer dispersion of graphene layers in ethanol due to insolubility of S-*g*-A(1.2) (Figure 3.6). After 72 hours standing under ambient condition, three nanocomposites (Gr/S-*g*-A(0.5), Gr/S-*g*-A(0.7), Gr/S-*g*-A(0.9)) retain dark purple color in ethanol without precipitation, indicating that the dispersion of graphenes in ethanol is very stable and not precipitated.

3.3. Examination of microstructure

The microstructure of Gr/S-*g*-A and Gr/CNT/S-*g*-A nanocomposites was observed by scanning electron microscopy (SEM) and transmission electron microscopy (TEM), as shown in Figure 3.7 and 3.8. In Figure 3.7a, it was observed that graphite is well exfoliated into graphene layers and S-*g*-A covers fully the surface of exfoliated graphene layer. Figure 3.7b shows the

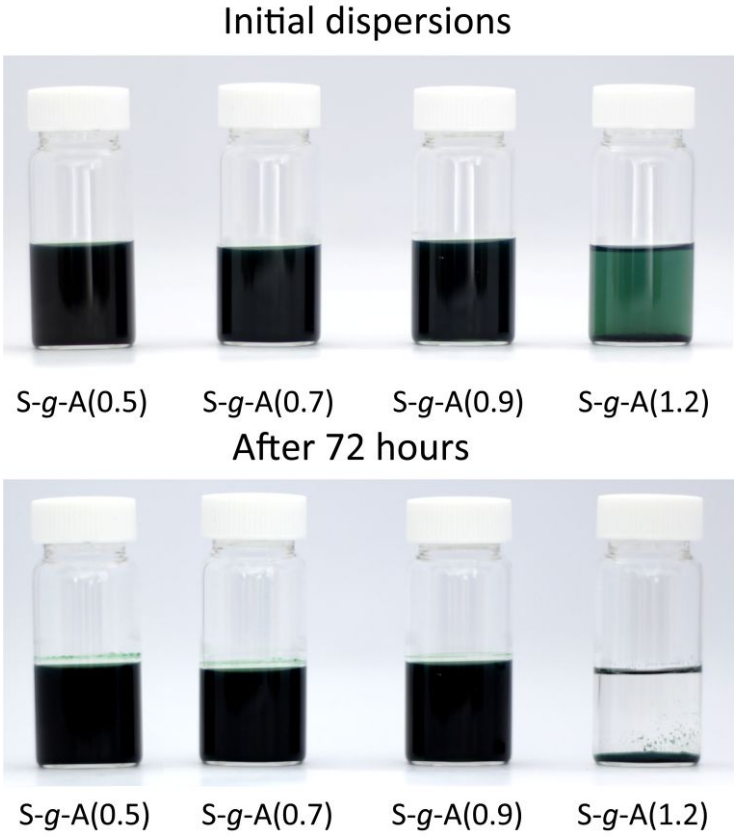

Figure 3.5 Comparison of dispersions of S-*g*-A(0.5), S-*g*-A(0.7), S-*g*-A(0.9), S-*g*-A(1.2).microstructure of Gr/CNT/S-*g*-A with well-dispersed MWCNT.

nanostructures of Gr/CNT/S-*g*-A with well-dispersed MWCNT. From these SEM images, it is found that dispersed MWCNT forms nanocomposites with exfoliated graphene and S-*g*-A. Figure 3.8 shows the nanostructure of the composites through TEM images. Exfoliated graphene was exhibited in

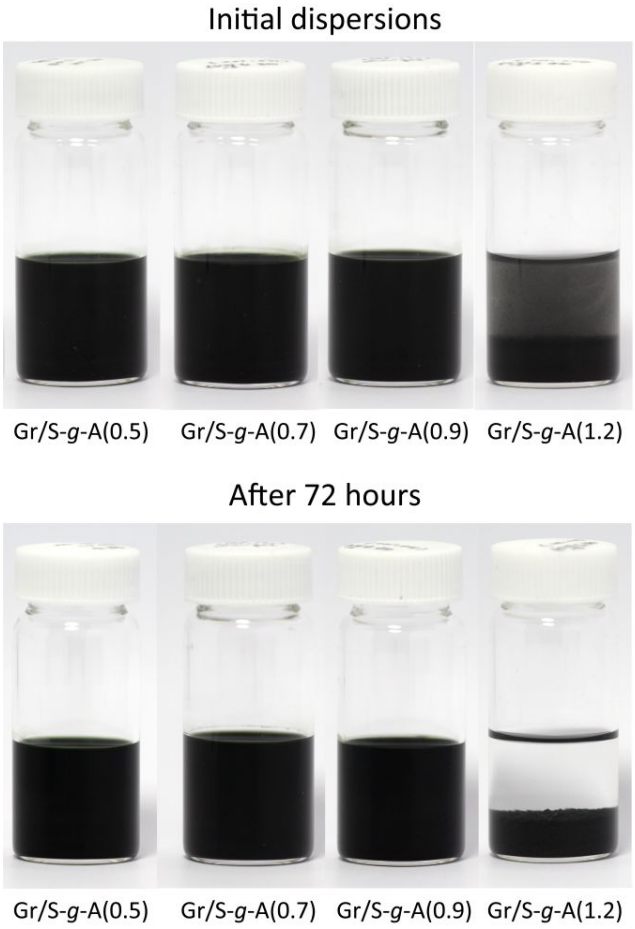

Figure 3.6 Comparison of graphene dispersions using S-*g*-A(0.5), S-*g*-A(0.7), S-*g*-A(0.9), S-*g*-A(1.2) in ethanol at initial mixing state and after 3 days standing.

Figure 3.8a. Besides, Gr/CNT/S-*g*-A nanocomposite was also shown in Figure 3.8b. By magnifying the TEM image of Gr/CNT/S-*g*-A nanocomposites (Figure 3.8b), the structure of multiwalled carbonnanotubes can be confirmed.

Furthermore, atomic force microscopic (AFM) analysis is another direct way to investigate the surface structure and thickness of Gr/S-*g*-A composite. When the thickness of Gr/S-*g*-A composite was estimated from the depth profile of AFM image (Figure 3.9), the thickness of the composite was measured from 2 scans (X, Y). Since the average height of the base line to the maximum point of the composite corresponds to the thickness of Gr/S-*g*-A composite (9.1 nm), and the thickness of S-*g*-A can be calculated (2.9 nm), the average thickness of graphene layers in the composite is 3.3 nm. From the thickness of graphene layers, it is clear that 2–3 layered graphenes are well dispersed in Gr/S-*g*-A(0.9) composite: The average thicknesses of S-*g*-A(0.9) and graphene layer are ca. 2.9 nm and 3.3 nm, respectively.

3.4. Identification of interaction

Raman spectroscopy analysis which is one of the effective methods to analyze the structure of nanocomposites was performed to investigate the structure of graphite, S-*g*-A and Gr/S-*g*-A nanocomposite. Figure 3.10 compares the Raman spectra of pristine graphite, S-*g*-A, and Gr/S-*g*-A. The Raman spectrum of S-*g*-A(0.9) shows the typical vibrational absorption bands of acid doped emeraldine salt, an electrically conducting form of polyaniline: 832 cm^{-1} (benzoid ring symmetric stretching; amine deformation), 887 cm^{-1} (benzoid ring deformation), 1170 cm^{-1} (C–H in-plane bending in quinoid ring), 1199 cm^{-1} (C–H in-plane bending in benzoid ring), 1258 and 1334 cm^{-1} ($C–N^{+}$ of the radical cation), 1510 cm^{-1} (C=N and CH=CH stretching in

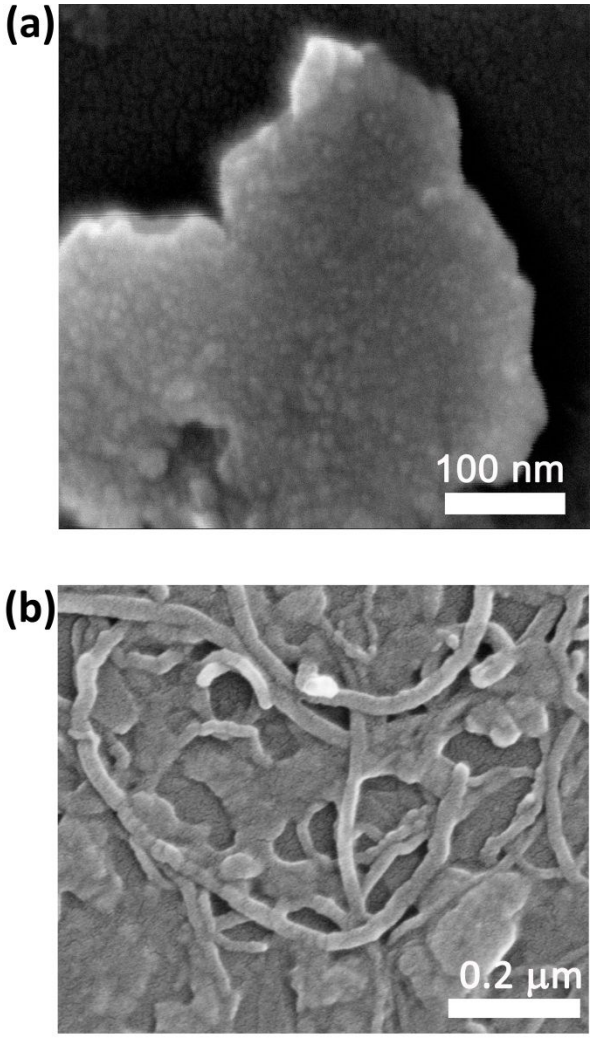

Figure 3.7 SEM image of (a) Gr/S-*g*-A(0.9) with fully exfoliated graphene layer covered with S-*g*-A and (b) Gr/CNT/S-*g*-A(0.9) with dispersed MWCNT

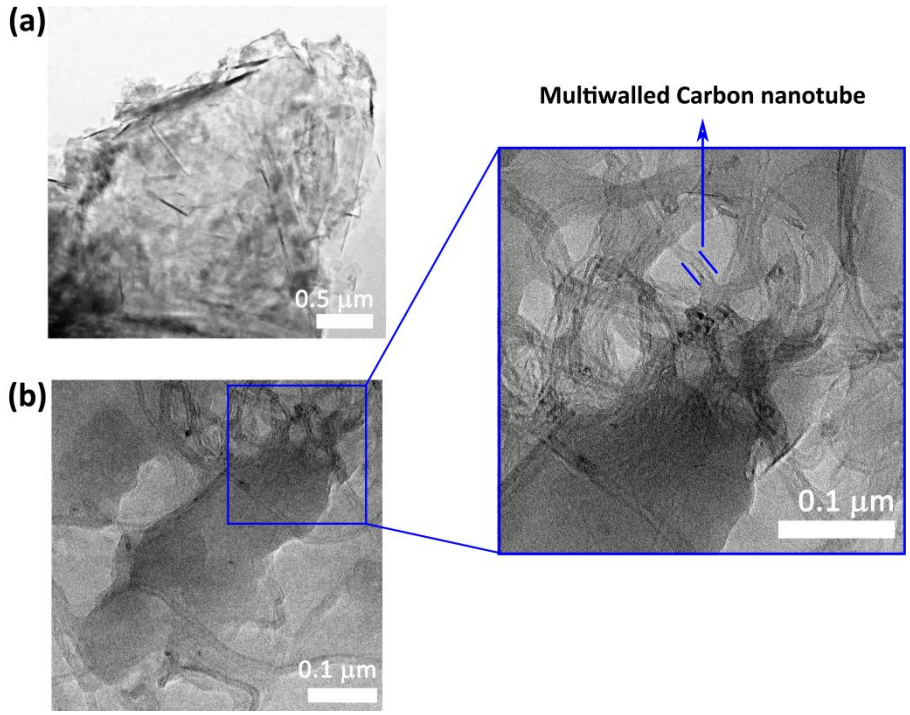

Figure 3.8 TEM images of (a) Gr/S-*g*-A(0.9) with fully exfoliated graphene layer covered with S-*g*-A and (b) Gr/CNT/S-*g*-A(0.9) with dispersed MWCNT.

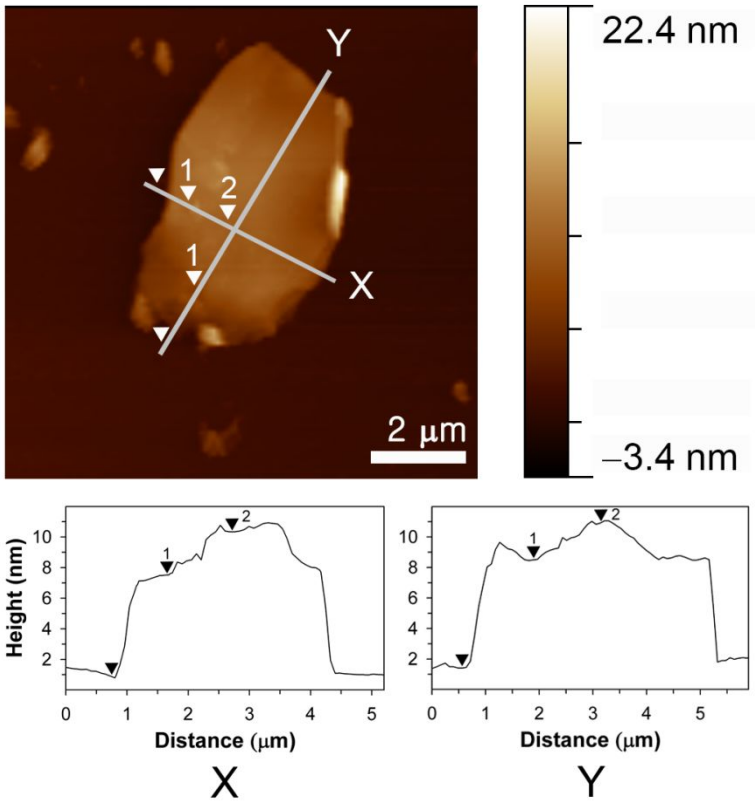

Figure 3.9 AFM images of Gr/S-*g*-A(0.9) with fully exfoliated graphene layer covered with S-*g*-A. The thickness of the composite was measured from 2 scans (X, Y). The average height of the base line to point 2 (9.1 nm) corresponds to the thickness of (S-*g*-A + graphene), and the height of point 1 to point 2 (2.9 nm) corresponds to the thickness of S-*g*-A. Hence, the average thickness of graphene layer is 3.3 nm (= 9.1 nm – 2 x 2.9 nm), since S-*g*-A is covered on both sides of graphene layer.

quinoid ring) and 1630 cm^{-1} (C–C stretching in benzoid ring).[26,27] Graphite exhibits 3 characteristic peaks of D band at 1359 cm^{-1}, G band at 1590 cm^{-1}, and 2D band at 2730 cm^{-1}.[28] As expected, the Raman spectrum of Gr/S-*g*-A(0.9) reveals all peaks arising from both graphite and S-*g*-A. However, one of noticeable changes in the spectrum of Gr/S-*g*-A nanocomposite is that D and G bands slightly shift to high frequencies due to the interaction between graphene and S-*g*-A as compared with the corresponding bands of pristine graphite.[24,29] Another noticeable change is that Gr/S-*g*-A(0.9) exhibits one broad 2D peak while graphite shows two peaks composed of one weak and one intense peak, indicating that single and bilayer graphenes are well dispersed in Gr/S-*g*-A (0.9).[30]

For identifying the structural change and chemical interaction between graphene and S-*g*-A, X-ray photoelectron spectra (XPS) of S-*g*-A(0.9) and Gr/S-*g*-A(0.9) were measured and compared (Figure 3.11). Comparing XPS survey spectra of S-*g*-A(0.9) and Gr/S-*g*-A(0.9) reveals no clear difference between two samples (Figure 3.11a), because the nanocomposites were prepared by simple exfoliation method without additional chemical treatment. However, when the high-resolution C 1s peak of Gr/S-*g*-A(0.9) is deconvoluted into five Gaussian peaks at 284.5, 284.8, 286.2, 286.9, and 290.2 eV, corresponding to the typical signals of sp^2-hybridized carbon,[24] sp^3-hybridized carbon,[27] C–N,[31] C–S[32] and C=O/O–C=O,[33] respectively, as containing functional groups (C=O and O–C=O) in addition to the peak derived from the functional groups of S-*g*-A(0.9), indicating that the S-*g*-A in the nanocomposite is oxidized to some extent due to reactive nature of

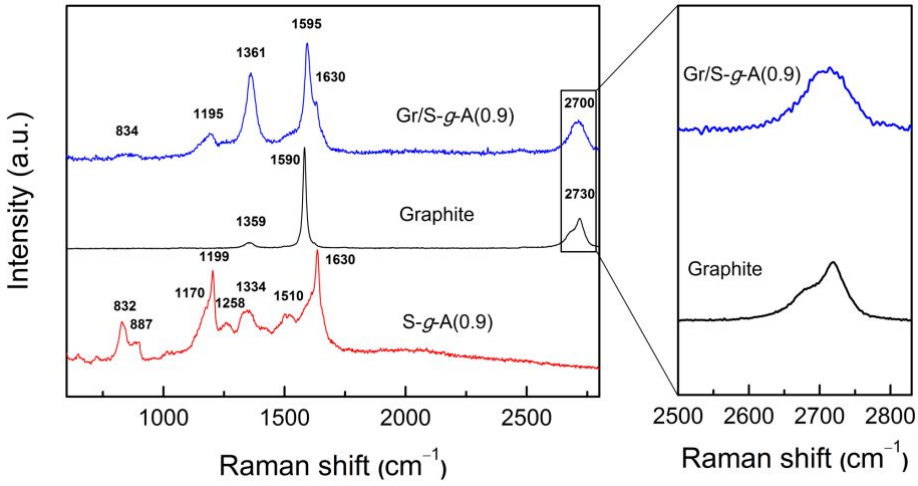

Figure 3.10 Comparison of Raman spectra of Gr/S-*g*-A, graphite and S-*g*-A(0.9)

conjugated polymer.[33] When the N 1s spectra of both S-*g*-A(0.9) and Gr/S-*g*-A(0.9) are deconvoluted into two peaks corresponding to benzenoid amine nitrogen (–NH–) and protonated nitrogen (N^+) centered at 399.6 eV and 401.5 eV,[34] respectively, it reveals that the relative fraction of protonated nitrogen atoms (65%) (Figure 3.11d) in Gr/S-*g*-A(0.9) is larger than that of S-*g*-A(0.9) (60%) (Figure 3.11c), indicating that strong π–π interaction between graphene and PANI exists in the composite.[35,36] From these interactions, it can be conferred that Gr/S-*g*-A nanocomposites would show higher conductivities and electrochemical performances than graphene and S-*g*-A respectively.

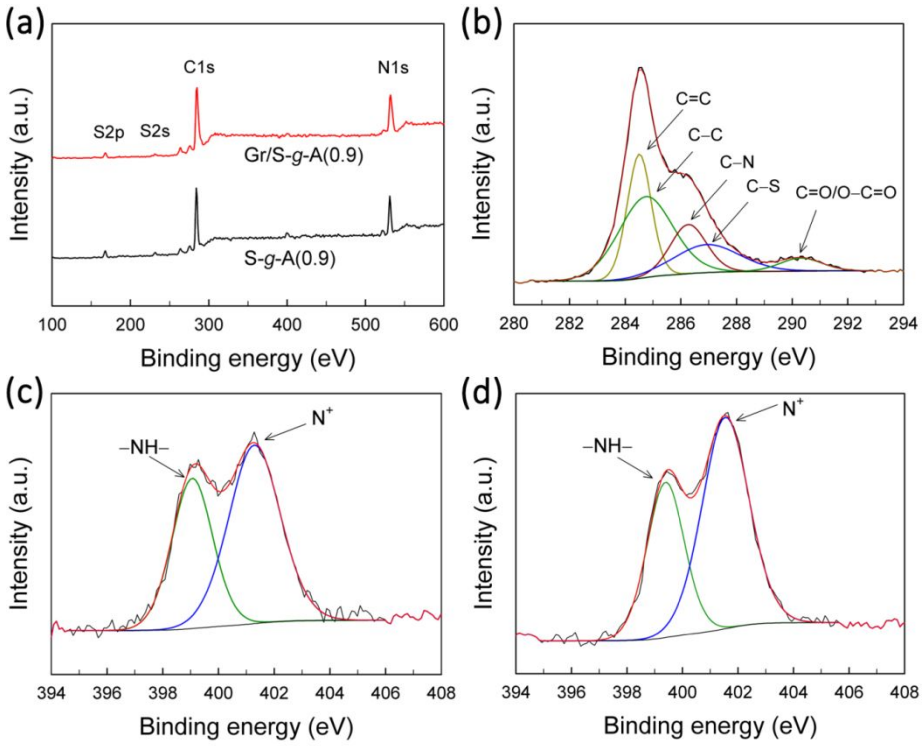

Figure 3.11 (a) XPS survey spectra of Gr/S-*g*-A(0.9) and S-*g*-A(0.9); (b) high-resolution C1s spectrum of Gr/S-*g*-A(0.9), high-resolution N1s spectra of (c) S-*g*-A(0.9), and (d) Gr/S-*g*-A(0.9).

3.5. Surface property

To identify the surface property of nanocomposite, N_2 adsorption-desorption was measured at 77 K for graphite, MWCNT, sonicated graphite in ethanol and the nanocomposites of Gr/S-*g*-A(0.9) and Gr/CNT/S-*g*-A(0.9). The results were listed in Table 3.2. As expected, pristine graphite shows the

lowest specific surface area of 1.74 m^2/g. Interestingly, the specific surface area of sonicated graphite in ethanol is higher than pristine graphite, implying that ethanol itself can also exfoliate graphite into graphenes to some extent under sonication.20 Compared to sonicated graphite, Gr/S-*g*-A(0.9) possesses 15 times larger surface area and 12 times larger total pore volume, indicating that S-*g*-A exfoliates graphite into few layers of graphene sheets and forms porous structure. Among the listed materials, Gr/CNT/S-*g*-A(0.9) exhibits the highest specific surface area of 214 m^2/g with total pore volume of 0.73 cm^3/g, even though a sum of the specific surface area of MWCNT and Gr/S-*g*-A is 164 m^2/g. It means that MWCNT in Gr/CNT/S-*g*-A nanocomposite acts as scaffolds for porous structure since MWCNTs have strong $\pi-\pi$ interaction with both graphene sheets and S-*g*-As leading to forming high surface area structure by synergy effect with graphene, S-*g*-A and MWCNT. By enhancing the specific surface area of Gr/CNT/S-*g*-A nanocomposite, the larger specific capacitance can be expected since more ion charges can be attached to large surface area.

3.6. Electrochemical properties

When the electrochemical properties of S-*g*-A(0.9) and Gr/CNT/S-*g*-A nanocomposites were measured by cyclic voltammetry (CV) with a potential window from 0.2 to 1.2 V, as shown in Figure 3.12, S-*g*-A(0.9) exhibits two broad peaks in the CV curve as measured at a scan rate of 50 mV/s, originated from two redox transitions of PANI corresponding to

Table 3.2 BET surface area and the total pore volume for graphite, sonicated graphite, Gr/S-*g*-A(0.9) and Gr/CNT/S-*g*-A(0.9).

Sample	S_{BET} (m^2/g)	V_T (cm^3/g)
Graphite	1.74	0.034
MWCNT	54	0.29
Sonicated graphite	7.13	0.04
Gr/S-*g*-A(0.9)	110	0.48
Gr/CNT/S-*g*-A(0.9)	214	0.73

leucoemeraldine/emeraldine and emeraldine/pernigraniline,[37] while the nanocomposite exhibits one broad peak in the CV curve. Since the CV curves of the nanocomposite show overall rectangular shapes with one broad peak, it is obvious that the composite has hybrid characteristics of EDLC and pseudocapacitance, leading to enhancement of capacitance due to combination of large surface area of graphene and MWCNT and high pseudocapacitance of PANI.[38] It is also noticeable that Gr/CNT/S-*g*-A(0.9) possesses the highest specific capacitance, as clearly shown by the largest integrated area of CV curve among those of other nanocomposites (Figure 3.12a). When the CV curves of Gr/CNT/S-*g*-A(0.9) are measured at different scan rate from 20 to 200 mV/s, it reveals that the anodic peak shifted positively while the cathodic peak shifted negatively due to the internal

resistance as the scan rate increases (Figure 3.12b).[39,40] When the specific capacitances were measured by cyclic voltammetry with different scan rate, the specific capacitances decreases from 509 F/g at 20 mV/s to 438 F/g at 200 mV/s. The decrease of capacitance with increase of scan rate is attributed to the fact that the redox reaction taking longer time cannot keep pace with the voltage change as the scan rate increases.[50,51]

When galvanostatic charge/discharge test was performed in order to further examine the capacitive properties of S-*g*-As and their nanocomposites, as shown in Figure 3.13, it was found that the composite exhibits nonlinear charge/discharge curve, indicating that the nanocomposites have pseudo-capacitive nature due to redox reaction of S-*g*-As. Another interesting feature to note is that S-*g*-A(0.9) exhibits significant IR drop of 0.4 V in discharge curve at a current density of 0.5 A/g due to high internal resistance whereas the nanocomposites do not exhibit discernible IR drop, indicating that the nanocomposites possess low internal and diffusion resistance. Especially, Gr/CNT/S-*g*-A(0.9) exhibits the specific capacitance of 531 F/g as measured at a current density of 0.5 A/g which is higher value than other graphene/CNT/PANI composites fabricated by other groups.[12,24,35,41-49] The larger capacitances of our nanocomposites can be explained by the followings: First, the covered S-*g*-A polymer on graphene sheets and MWCNT greatly shorten the diffusion path of electrolyte ion, leading to better utilization of active materials.[41] Second, the π–π interaction among PANI /graphene, PANI/MWCNT and graphene/MWCNT facilitates the electron transfer and reduces the contact resistance between the composite and working electrode.[24]

Lastly, non-defective graphene with high electrical conductivity produced by direct exfoliation method acts as effective conducting pathway. These facts reduce the total resistance of the electrode as evidenced by negligible IR drop of the nanocomposites and thus improve the specific capacitance. When the charge/discharge curves of Gr/S-*g*-A(0.9) were measured at different current densities of 0.2 to 2 A/g and the specific capacitance at each current density was calculated for further comparison of the capacitive properties, as shown in Figure 3.13b and 3.13c, it was observed that the specific capacitance of Gr/CNT/S-*g*-A(0.9) is 531 F/g at the current density of 0.5 A/g while it decreases to 443 F/g as the current density increases to 4 A/g. The decrease of capacitance with increase of current density is attributed to the fact that the redox reaction taking longer time as compared to EDLC cannot keep pace with the current flow as the current density increases as mentioned before.[50,51]

3.7. Electrochemical stability properties

The electrochemical stability of Gr/CNT/S-*g*-A nanocomposite electrode was evaluated by measuring the galvanostatic charge/discharge cycling at a current density of 20 A/g (Figure 3.14) for 5000 cycles of charging/discharging repetition. It has generally been known that PANI-based supercapacitors suffer from poor cycling stability because of swelling and shrinking of the polymer backbone during charging/discharging process, which cause degradation of the composite during cycle process.[52-56] Although the copolymer [S-*g*-A(0.9)] itself shows low capacitance retention (41% of

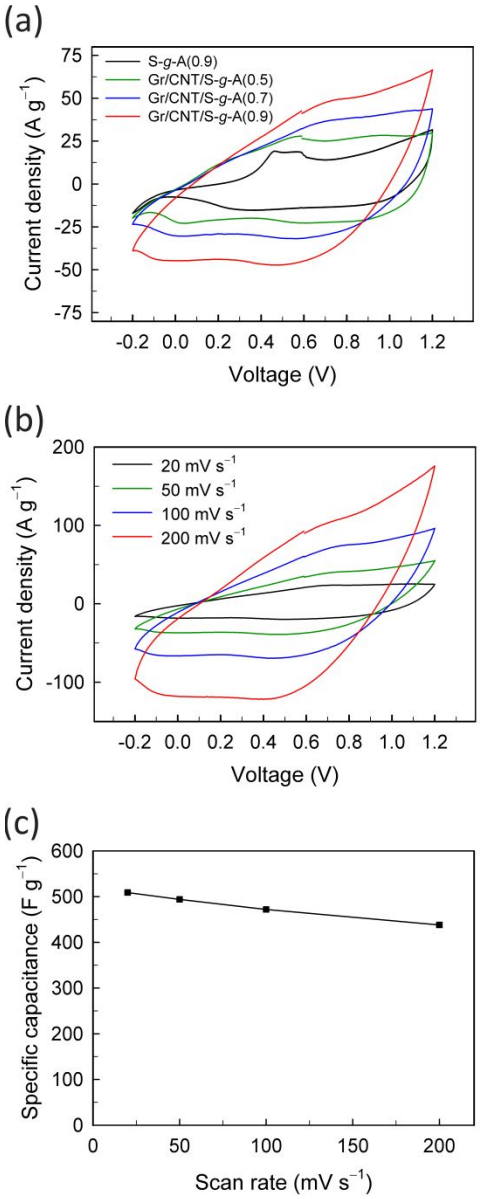

Figure 3.12 CV curves of (a) the nanocomposites and S-*g*-A at 50 mV/s, (b) Gr/CNT/S-*g*-A(0.9) at different scan rate, (c) variation of the specific capacitance with scan rate for Gr/CNT/S-*g*-A(0.9).

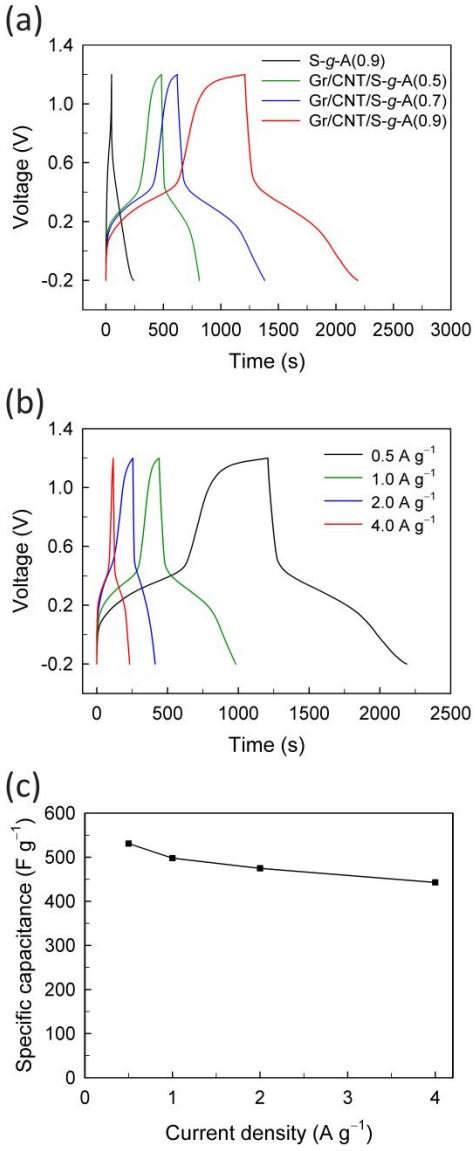

Figure 3.13 Galvanostatic charge/discharge curves of (a) the nanocomposites and S-*g*-A at a current density of 0.5 A/g, (b) Gr/CNT/S-*g*-A(0.9) at different current denstiy, (c) variation of the specific capacitance with current denstiy for Gr/CNT/S-*g*-A(0.9).

initial capacitance) after 5000 cycles (Figure 3.14a), the nanocomposite [Gr/CNT/S-*g*-A(0.9)] exhibits a high capacitance retention of 91% after 5000 cycles, which is comparable to those of other graphene/PANI and graphene/CNT/PANI nanocomposites fabricated by other methods including layered graphene/PANI film (84% retention after 1000 cycles),[24] graphene/PANI composite paper (82% retention after 1000 cycles),[17] re-doped PANI/reduced graphene composite (74% retention after 500 cycles)[35] and porous graphene/CNT/PANI hybrid paper (85% retention after 1000 cycles).[57] The improved cycle life of the nanocomposite is originated from larger surface area due to well exfoliated graphene layers and well dispersed MWCNTs in the nanocomposite, which can accommodate swelling and shrinking of polymer backbone during cycles preventing the polymer from degradation.[55,56]

3.8. Energy density and power density properties

Another important property for determining the supercapacitor performance is its specific energy and power density. The Ragone plot (energy density vs. power density) for Gr/CNT/S-*g*-A(0.9) nanocomposite based on total weight of electroactive materials is shown with the results of other supercapacitors for comparison in Figure 3.15. The nanocomposite (Gr/CNT/S-*g*-A(0.9)) exhibits its maximum energy density of 145 Wh/kg with a power density of 533 W/kg at a current density of 0.5 A/g (Table 3.3). These high values are attributed to low internal resistance confirmed from galvanostatic curves.

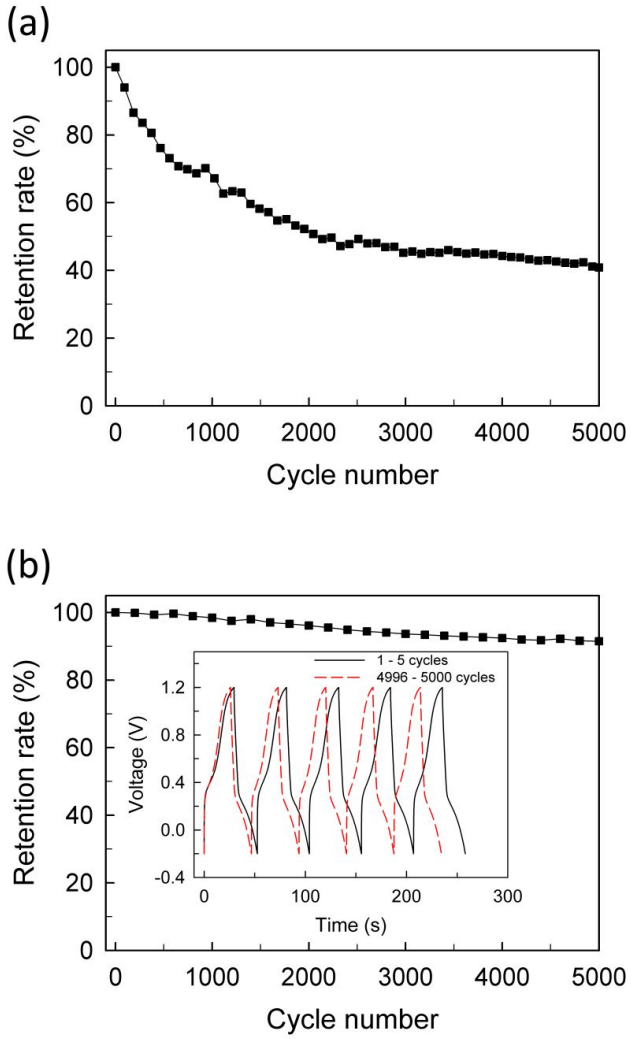

Figure 3.14 Cyclic stability of (a) S-*g*-A(0.9) and (b) Gr/CNT/S-*g*-A(0.9) during 5000 cycles of charging/discharging process at a current density of 20 A/g with the inset showing the first 5 cycles and the last 5 cycles.

Furthermore, the energy density does not decrease largely, exhibiting the energy density of 121 Wh/kg when the power density increases up to 3821 W/kg at a current density of 4 A/g, which is favorable for the high power delivery in practical applications. These values are much higher than those of other reported graphene/PANI and graphene/CNT/PANI composites: covalently-grafted PANI/GO composite (9.6 Wh/kg; 3468 W/kg),[18] PANI/boron-doped graphene composite (30.1 Wh/kg; 523.5 W/kg),[34] graphene/PANI composite (37.9 Wh/kg; 141.1 W/kg),[42] the wavy shaped PANI/graphene composite (23.2 Wh/kg; 399 W/kg),[45] sandwiched graphene/porous carbon composite (25.7 Wh/kg; 100 W/kg),[47] and PANI/sulfonated-graphene/CNT nanocomposite (41.5 Wh/kg; 167 W/kg).[58] These results demonstrate that the Gr/CNT/S-*g*-A composite prepared by direct exfoliation of graphite and dispersion of MWCNT exhibits superior electrochemical properties due to the unique hierarchical structure with well-exfoliated graphenes and well-dispersed MWCNT in the composite. Based on these advantages, Gr/CNT/S-*g*-A nanocomposite is expected to greatly boost the development of advanced energy storage devices applied in consumer electronics and electrical vehicles.

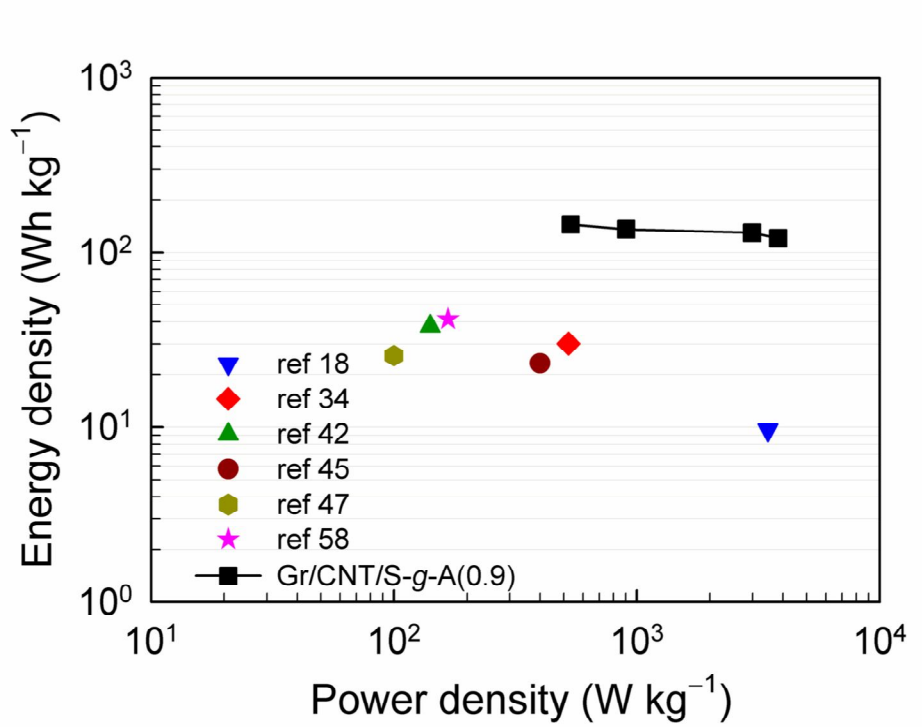

Figure 3.15 Ragone plot of Gr/CNT/S-*g*-A(0.9) and other PANI-based composites (covalently-grafted PANI/GO composite;[18] PANI/boron-doped graphene composite;[34] graphene/PANI composite;[41] the wavy shaped PANI/graphene composite;[45] sandwiched graphene/porous carbon composite;[47] PANI/sulfonated-graphene/CNT nanocomposite[58]).

Table 3.3 Electrochemical properties of the composites.

Sample	σ_{elec}[a] (S/cm)	Specific capacitance[b] (F/g)	Energy density[b] (Wh/kg)	Power density[b] (W/kg)
Gr/CNT/S-*g*-A(0.9)	5.31×10^{-1}	531	145	534
Gr/CNT/S-*g*-A(0.7)	3.48×10^{-1}	413	113	536
Gr/CNT/S-*g*-A(0.5)	2.46×10^{-1}	273	75	628
S-*g*-A(0.9)	1.31×10^{-1}	159	43.3	779.4

[a]σ_{elec} is electrical conductivity; [b]The electrochemical data were measured at a current density of 0.5 A/g

4. Conclusions

Gr/CNT/S-*g*-A nanocomposites were in-situ prepared through direct exfoliation of graphite and dispersion of MWCNT using polymeric surfactant (S-*g*-A) and applied to supercapacitor electrode. The direct exfoliation not only produces high quality graphene without extra process, but also forms in-situ the nanocomposite during the exfoliation process. When S-*g*-A with the molar ratio of ANI to SSA (0.9:1.0, the maximum ANI content that makes the copolymer soluble in ethanol) is used for exfoliation of graphite and dispersion of MWCNT, the resulting Gr/CNT/S-*g*-A nanocomposite exhibits the highest specific capacitance of 531 F/g at a current density of 0.5 A/g and the energy density of 145 Wh/kg at a power density of 534 W/kg. Furthermore, the nanocomposite retains 91% of its initial capacitance after 5000 cycles, indicating high electrochemical cyclic stability. In short, the direct exfoliation of graphite and dispersion of MWCNT using conductive polymer as a surfactant provides a promising method for development of high-performance electrode materials in energy storage devices.

Bibliography

(1) P. Simon, Y. Gogotsi, *Nat. Mater.* **2008,** *7*, 845.

(2) W. Guoping, Z. Lei, Z. Jiujin, *Chem. Soc. Rev.* **2012,** *41*, 797.

(3) L. L. Zhang, X. S. Zhao, *Chem. Soc. Rev.* **2009,** *38*, 2520.

(4) C. Hu, L. Song, Z. Zhang, N. Chen, Z. Feng, L. Qu, *Energy Environ. Sci.* **2015,** *8*, 31.

(5) X. Wang, C. Yan, A. Sumboja, J. Yan, P. S. Lee, *Adv. Energy Mater.* **2014,** *4*, 1301240

(6) H. Gao, F. Xiao, C. B. Ching, H. Duan, *ACS Appl. Mater. Interfaces* **2012,** *4*, 7020.

(7) K. S. Novoselov, A. K. Geim, S. V. Morozov, D. Jiang, Y. Zhang, S. V. Dubonos, I. V. Grigorieva and A. A. Firsov, *Science* **2004,** *306*, 666.

(8) A. K. Geim and K. S. Novoselov, *Nat. Mater.* **2007,** *6*, 183

(9) C. Lee, X. Wei, J. W. Kysar and J. Hone, *Science* **2008,** *321*, 385.

(10) A. Peigney, C. Laurent, E. Flahaut, R. R. Bacsa and A. Rousset, *Carbon* **2001,** *39*, 507.

(11) A. A. Balandin, S. Ghosh, W. Bao, I. Calizo, D. Teweldebrhan, F. Miao and C. N. Lau, *Nano Lett.* **2008,** *8*, 902.

(12) H.-P. Cong, X.-C. Ren, P. Wang, S.-H. Yu, *Energy Environ. Sci.*

2013, *6*, 1185.1392.

(13) B. C. Kim, J. Y. Hong, G. G. Wallace, H. S. Park, *Adv. Energy Mater.* **2014,** DOI: 10.1002/aenm.201500959

(14) H. Li, J. Wang, Q. Chu, Z. Wang, F. Zhang, S. Wang, *J. Power Sources* **2009,** *190*, 578.

(15) L. Lai, H. Yang, L. Wang, J. Zhong, H. Chou, L. Chen, W. Chen, Z. Shen, R. S. Ruoff, J. Lin, *ACS Nano* **2012,** 6, 5941.

(16) L. Wang, X. Lu, S. Lei, Y. Song, *J. Mater. Chem. A* **2014,** *2*, 4491.

(17) K. Zhang, L. L. Zhang, X. S. Zhao, J. Wu, *Chem. Mater.* **2010,** *22*, 1392.

(18) Z.-F. Li, H. Zhang, Q. Liu, Y. Liu, L. Stanciu, J. Xie, *Carbon* **2014,** *71*, 257.

(19) D.-W. Wang, F. Li, J. Zhao, W. Ren, Z.-G. Chen, J. Tan, Z.-S. Wu, I. Gentle, G. Q. Lu, H.-M. Cheng, *ACS Nano* **2009,** *3*, 1745.

(20) X. An, T. Simmons, R. Shah, C. Wolfe, K. M. Lewis, M. Washington, S. K. Nayak, S. Talapatra, S. Kar, *Nano Lett.* **2010,** *10*, 4295.

(21) G. Eda, G. Fanchini, M. Chhowalla, *Nat Nano.* **2008,** *3*, 270.

(22) M. Lotya, Y. Hernandez, P. J. King, R. J. Smith, V. Nicolosi, L. S. Karlsson, F. M. Blighe, S. De, Z. Wang, I. T. McGovern, G. S. Duesberg, J. N. Coleman, *J. Am. Chem. Soc.* **2009,** *131*, 3611.

(23) W. J. Bae, K. H. Kim, Y. H. Park, W. H. Jo, *Chem. Commun.* **2003,** *22*,

2768.

(24) Z. Tong, Y. Yang, J. Wang, J. Zhao, B.-L. Su, Y. Li, *J. Mater. Chem. A* **2014,** *2*, 4642.

(25) D. Rangappa, K. Sone, M. Wang, U. K. Gautam, D. Golberg, H. Itoh, M. Ichihara, I. Honma, *Chem. Eur. J.* **2010,** *16*, 6488.

(26) T. Lindfors, A. Ivaska, *J. Electroanal. Chem.* **2005,** *580*, 320.

(27) T. Lindfors, R.-M. Latonen, *Carbon* **2014,** *69*, 122.

(28) M. Cai, D. Thorpe, D. H. Adamson, H. C. Schniepp, *J. Mater. Chem.* **2012,** *22*, 24992.

(29) Q. Zhou, Y. Li, L. Huang, C. Li, G. Shi, *J. Mater. Chem. A* **2014,** *2*, 17489.

(30) A. C. Ferrari, J. C. Meyer, V. Scardaci, C. Casiraghi, M. Lazzeri, F. Mauri, S. Piscanec, D. Jiang, K. S. Novoselov, S. Roth, A. K. Geim, *Phys. Rev. Lett.* **2006,** *97*, 187401.

(31) H. Bai, Y. Xu, L. Zhao, C. Li, G. Shi, *Chem. Commun.* **2009,** *13*, 1667.

(32) M. Islam, A. Chidembo, H. Aboutalebi, D. Cardillo, H. K. Liu, K. Konstantinov, S. X. Dou, *Front. Energy Res.* **2014,** *2*, 31.

(33) Y. Chen, E. T. Kang, K. G. Neoh, S. L. Lim, Z. H. Ma, K. L. Tan, *Colloid Polym. Sci.* **2001,** *279*, 73.

(34) Q. Hao, X. Xia, W. Lei, W. Wang, J. Qiu, *Carbon* **2015,** *81*, 552.

(35) M. Kim, C. Lee, J. Jang, *Adv. Funct. Mater.* **2014,** 24, 2489.

(36) S. Cho, J. Lee, S. Kim, J. Jang, *Nanoscale* **2014,** *6*, 15181

(37) J. Xu, K. Wang, S.-Z. Zu, B.-H. Han, Z. Wei, *ACS Nano* **2010,** *4*, 5019.

(38) L. Z. Fan, Y. S. Hu, J. Maier, P. Adelhelm, B. Smarsly, M. Antonietti, *Adv. Funct. Mater.* **2007,** *17*, 3083.

(39) Q. Wang, J. Yan, Z. Fan, T. Wei, M. Zhang, X. Jing, *J. Power Sources* **2014,** *247*, 197.

(40) Y. G. Wang, H. Q. Li, Y. Y. Xia, *Adv. Mater.* **2006,** *18*, 2619.

(41) H. Mi, J. Zhou, Q. Cui, Z. Zhao, C. Yu, X. Wang, J. Qiu, *Carbon* **2014,** *80*, 799.

(42) H. Wang, Q. Hao, X. Yang, L. Lu, X. Wang, *Nanoscale* **2010,** *2*, 2164.

(43) J. Yan, L. Yang, M. Cui, X. Wang, K. J. Chee, V. C. Nguyen, V. Kumar, A. Sumboja, M. Wang, P. S. Lee, *Adv. Energy Mater.* **2014,** *4*, 1400781.

(44) L. Liu, Z. Niu, L. Zhang, W. Zhou, X. Chen, S. Xie, *Adv. Mater.* **2014,** *26*, 4855.

(45) Y. Xie, Y. Liu, Y. Zhao, Y. H. Tsang, S. P. Lau, H. Huang, Y. Chai, *J. Mater. Chem. A* **2014,** *2*, 9142.

(46) S. Zhou, H. Zhang, Q. Zhao, X. Wang, J. Li, F. Wang, *Carbon* **2013,** *52*, 440.

(47) J. Yan, Q. Wang, C. Lin, T. Wei, Z. Fan, *Adv. Energy Mater.* **2014,** 98,

1400500.

(48) Z.-F. Li, H. Zhang, Q. Liu, L. Sun, L. Stanciu, J. Xie, *ACS Appl. Mater. Inter.* **2013,** *5*, 2685.

(49) H. Fan, N, Zhao, H. Wang, J. Xu, F. Pan, *J. Mater. Chem. A* **2014,** *2*, 12340.

(50) W.-W. Liu, Y.-Q. Feng, X.-B. Yan, J.-T. Chen, Q.-J. Xue, *Adv. Funct. Mater.* **2013,** *23*, 4111.

(51) X. Li, B. Wei, *Nano Energy* **2012,** *1*, 479.

(52) L. Wang, L. Chen, B. Yan, C. Wang, F. Zhu, X. Jiang, Y. Chao, G. Yang, *J. Mater. Chem. A* **2014,** *2*, 8334.

(53) J. Yan, T. Wei, Z. Fan, W. Qian, M. Zhang, X. Shen, F. Wei, *J. Power Sources* **2010,** *195*, 3041.

(54) I. Kovalenko, D. G. Bucknall, G. Yushin, *Adv. Funct. Mater.* **2010,** *20*, 3979.

(55) L. Mao, K. Zhang, H. S. On Chan, J. Wu, *J. Mater. Chem.* **2012,** *22*, 80.

(56) G. Lota, K. Fic, E. Frackowiak, *Energy Environ. Sci.* **2011,** *4*, 1592.

(57) W. Fan, Y.-E. Miao, L. Zhang, Y. Huang and T. Liu, *RSC Adv.* **2015,** *5*, 31064

(58) J. Shen, C. Yang, X. Li, G. Wang, *ACS Appl. Mater. Interfaces* **2013,** *5*, 8467

초 록

S-*g*-A를 합성하여 계면활성제로 활용하여 흑연을 직접 박리시키고 다중벽 탄소나노튜브를 분산시킴으로써 그래핀/탄소나노튜브/S-*g*-A 나노복합체를 만들어 이를 슈퍼커패시터 전극으로 활용한 연구이다. S-*g*-A의 경우 PANI와 SSA의 구성비를 달리하여 합성하여 각각 흑연의 박리 및 다중벽 탄소나노튜브 분산제로 활용하였다. 이 복합체 및 고분자의 용매에 대한 분산정도는 디지털 카메라를 통해 확인하였고, SEM과 TEM 이미지를 통해 그래핀 및 복합체의 미세구조를 관찰하였다. 또한 AFM을 통한 두께 측정을 통해 박리된 그래핀의 두께를 확인하였다. 이렇게 박리된 그래핀은 raman spectroscopy를 통해 1~2 층의 그래핀으로 박리되어 있는 것을 확인하였고, X-ray photoelectron spectroscopy를 통해 그래핀 및 다중벽 탄소나노튜브와 S-*g*-A 간의 상호영향도 역시 확인하였다. 또한 나노복합체의 단위 표면적 측정을 위해 BET 표면 측정법을 활용하여 각 물질의 단위 표면적을 측정하였고 이를 통해 그래핀/탄소나노튜브/S-*g*-A의 단위 표면적이 가장 큰 것을 확인함으로써 슈퍼커패시터 전극 물질로써의 특징을 확인하였다. 최종적으로 복합체의 전기화학적 성능을 평가하기 위해 cyclic voltammetry 방법과 galvanostatic charging/discharging 시험을 진행하였다. 그 결과 0.5 A/g의 전류밀도에서 531 F/g 이라는 높은 값의 커패시턴스 값을 나타내었고 이는 기존 그래핀/탄소나노튜브/폴리아닐린 복합체들보다 높은 수치인 것을

확인하였다. 뿐만 아니라 동일한 전류밀도에서 145 Wh/kg의 에너지 밀도와 534 W/kg의 출력 밀도를 나타내어 다른 그래핀/폴리아닐린 복합체와 그래핀/탄소나노튜브/폴리아닐린 복합체들보다 높은 수치를 나타내었다. 안정성 실험에서 역시 20 A/g의 전류밀도에서 5000번의 충방전 순환을 하였을 때 초기 커패시턴스 대비 약 91%의 보존 수치를 보였다.

결론적으로 이 연구에서는 S-*g*-A를 이용한 흑연의 직접박리 및 다중벽 탄소나노튜브 분산을 통해 그래핀/탄소나노튜브/S-*g*-A 나노복합체를 만들어 슈퍼커패시터 전극으로 활용하여 531 F/g의 높은 커패시턴스를 얻어 미래의 에너지 저장 장치에 사용될 수 있는 고효율 전극 소재로 활용 가능할 것으로 기대된다.

주요어: 그래핀, 폴리아닐린, 탄소나노튜브, 슈퍼커패시터, 직접 박리
학 번: 2014-21438